Promoter effect of Ga in Pt/Ga-TiO$_2$ catalysts for the photo-production of H$_2$ from aqueous solutions of ethanol

A.C. Sola [a,b], M. Broch Gösser [a], P. Ramírez de la Piscina [a], N. Homs [a,b,*]

[a] Departament de Química Inorgànica i Orgànica, secció de Química Inorgànica, and Institut de Nanociència i Nanotecnologia, Universitat de Barcelona, Martí i Franquès 1-11, 08028 Barcelona, Spain
[b] Catalonia Institute for Energy Research (IREC), Jardins de les Dones de Negre 1, 08930 Barcelona, Spain

A B S T R A C T

In this paper, the effect of Ga in Pt/Ga-TiO$_2$ catalysts for photocatalytic H$_2$ production from aqueous solutions of ethanol is studied. The fresh and post-reaction catalysts were characterized using different techniques including BET, XRD, TPR, SEM-EDX, XPS, CO chemisorption and in situ DRIFTS. The presence of Ga in Pt/TiO$_2$-based catalysts increased the Pt dispersion and decreased the relative amount of surface oxidized Pt species. Pt/Ga-TiO$_2$ catalysts showed more stable behaviour during the photocatalytic reaction than the reference Pt/TiO$_2$. The Pt/0.2Ga-TiO$_2$ catalyst showed a higher initial rate of production of H$_2$ and produced a higher total amount of H$_2$ than the monometallic Pt/TiO$_2$. The promoter effect of Ga is analysed in the light of the surface characteristics of the catalysts.

© 2017 Elsevier B.V. All rights reserved.

1. Introduction

The use of photocatalytic processes to produce H$_2$ from aqueous solutions of bio-alcohols is of great interest in the energy context [1–4]. Ethanol is currently the bio-fuel produced in the largest quantities worldwide. Much work has been devoted to the study of the use of ethanol as a sacrificial agent for the photocatalytic production of H$_2$ using Pt/TiO$_2$ [5–10]. Ethanol is oxidized and the photogenerated h$^+$ are consumed, while H$^+$ is reduced to H$_2$ at the metal sites where the electrons are trapped, inhibiting the h$^+$/e$^-$ recombination [11]. The presence of dopants could improve the photocatalytic behaviour of Pt/TiO$_2$ catalysts, due to modification of the TiO$_2$ or of Pt nanoparticles. However, although the modification of TiO$_2$ produced by the presence of dopants is often studied in depth, the influence of the dopants on the characteristics of Pt nanoparticles is normally ignored. If the characteristics of Pt nanoparticles are modified, the Pt-TiO$_2$ interface that may play a main role in the photocatalytic behaviour of Pt/TiO$_2$, could also change [3,12,13]. The presence of Ga in TiO$_2$ has been shown to enhance the photocatalytic behaviour of the original TiO$_2$. This effect has been related with the generation of oxygen vacancies and defect levels near the conduction band in TiO$_2$, which can trap electrons and avoid h$^+$/e$^-$ recombination [14,15]. Initial work carried out by our group demonstrated that the introduction of Ga into Pt/SiO$_2$ catalysts decreases the particle size of the Pt and changes its catalytic behaviour, minimizing activity in reactions catalysed by ensembles of Pt [16]. We have also found that the presence of Ga in Cu-based catalysts can increase the Cu dispersion and the stability of the catalysts in hydrogenation of CO$_2$ to methanol [17]. One could expect that the presence of Ga would modify the Pt nanoparticles and consequently the photocatalytic behaviour of Pt/TiO$_2$. The aim of the current work is to study the effect of the addition of Ga to the Pt/anatase catalysts used in the photocatalytic production of H$_2$ from ethanol$_{(aq)}$. To this end, Pt/Ga-TiO$_2$ catalysts with a Pt content of some 0.5%wt and a Ga content in the range 0–1.3%wt were prepared and tested in photocatalytic production of H$_2$ from ethanol$_{(aq)}$ (25% v/v) for 24 h. The characteristics of both the TiO$_2$ and Pt nanoparticles, which were determined before and after the photocatalytic test, were used to analyse the photocatalytic behaviour.

2. Experimental

2.1. Preparation and characterization of the catalysts

Pt/aGa-TiO$_2$ (where a = Ga%wt) catalysts were prepared by successive incipient wetness impregnation using a previously studied TiO$_2$ anatase (Sigma Aldrich) [18] and aqueous solutions of both

* Corresponding author at: Departament de Química Inorgànica i Orgànica, secció de Química Inorgànica, and Institut de Nanociència i Nanotecnologia, Universitat de Barcelona, Martí i Franquès 1-11, 08028 Barcelona, Spain.
    E-mail addresses: narcis.homs@qi.ub.edu, nhoms@irec.cat (N. Homs).

$Ga(NO_3)_3 \cdot xH_2O$ and $H_2PtCl_6 \cdot 6H_2O$. First, the Ga precursor was impregnated and then the solid was dried at 353 K and calcined at 673 K (30 min); in a second step, the Pt was impregnated with a subsequent drying at 353 K and calcination at 673 K (4 h). The Pt/TiO_2 catalyst was prepared in a similar manner but without the incorporation of Ga [19].

The Pt and Ga content of the catalysts was determined by inductively-coupled plasma (ICP) atomic emission spectrometry using a Perkin Elmer Optima 3200RL.

N_2 adsorption desorption BET isotherms at 77 K were used to determine the surface area (S_{BET}), pore volume (V_{pore}) and pore diameter (D_{pore}) of the photocatalyst with a Micromeritics TriStar II 3020 system.

Band-gap values were determined by UV–vis diffuse reflectance spectroscopy. The reflectance spectra were collected using a Perkin Elmer Lambda 950 UV/vis Spectrometer with a 3 nm slit width and a speed of 654.92 nm min^{-1}; and using $BaSO_4$ as the reference.

An Xpert PRO-diffractometer equipped with a CuKα radiation source ($\lambda = 1.5406$ Å) and a graphite monochromator was used to perform the XRD analysis. The XRD patterns were collected between $2\theta = 10°$ and $2\theta = 100°$, with a step width of 0.05°, counting 3 s at each step. The mean TiO_2 crystallite size was estimated using the Scherrer equation.

Raman spectra were recorded with a Jobin-Yvon LabRam HR 800 spectrometer in micro-Raman mode using a 532 nm solid-state laser (visible-Raman), whose power was limited to 1.5 mW. The spectrometer was equipped with a CCD detector coupled to an Olympus BXFM optical microscope. Spectra were acquired using 3 accumulations of 5 s each. The samples were studied at 50× magnification.

X-ray photoemission spectra were recorded with a Perkin Elmer PHI-5500 spectrometer equipped with an Al Kα source (1486.6 eV) and a hemispherical analyser, maintaining the pressure in the analysis chamber below 10^{-8} torr during data acquisition. Binding energy (BE) values were referenced to the adventitious C 1 s peak at 284.8 eV.

SEM images were obtained using a ZEISS Auriga microscope equipped with an energy-dispersive X-ray detector at 20 kV to analyse the local chemical composition.

H_2-TPR analysis and CO chemisorption experiments were performed using a Micromeritics Autochem II 2920 system. For the H_2-TPR experiments, the samples were treated with a 10% (v/v) H_2/Ar flow from 253 K to 973 K, increasing the temperature at 10 K min^{-1}. CO chemisorption was carried out at 308 K. Before the experiments, the samples were reduced at 398 K under a 10% (v/v) H_2/Ar stream for 45 min and then purged with He for a further 30 min at 398 K.

CO species adsorbed onto the catalysts were followed by in situ diffuse reflectance infrared spectroscopy (DRIFTS). A Nicolet Magna-IR 750 FTIR spectrometer equipped with a liquid nitrogen-cooled MCT detector and a Spectra Tech catalytic chamber was used. The spectra recorded consisted of 128 scans at a spectral resolution of 2 cm^{-1}. Before CO adsorption, the samples were treated under a He flow (20 cm^3 min^{-1}) at 393 K for 30 min, and then cooled to 298 K. A 10%, v/v CO/He flow was brought into contact with the samples at 298 K for 15 min and then the samples were outgassed with He at the same temperature and the spectra were recorded.

2.2. Photocatalytic experiments

Photocatalytic tests were performed at 298 K using a jacketed reactor of 300 cm^3 capacity with an inlet and an outlet opening for gases and a 175 W Hg lamp (broad spectrum lamp, maximum power at $\lambda = 366$ nm: 25.6 W), placed inside the reactor in a water-cooled quartz jacket. 0.5 g of the catalysts and 250 cm^3 of ethanol$_{(aq)}$ (25% v/v) were used in all cases. The suspension was magnetically stirred and flushed with 24 cm^3 min^{-1} of N_2/Ar (40% v/v) before and during the experiments. The gaseous products were periodically sampled and analysed by a micro chromatograph Varian CP-4900 equipped with two columns, a molecular sieve (5 Å, 10 m) and a PPQ (10 m). N_2 in the flushing gas was used as an internal standard for the quantification of the gaseous products. The liquid products were sampled at the end of the reaction and analysed by gas chromatography and IR-ATR spectroscopy.

3. Results and discussion

3.1. Characterization of the fresh catalysts

Table 1 shows the $Pt/Ga-TiO_2$ catalysts studied in this work; their Pt content was approximately 0.5%wt and their Ga content was in the range 0.2–1.3%wt. The Pt/TiO_2 catalyst, which had previously been studied in the photocatalytic production of hydrogen from ethanol$_{(aq)}$ [19], is also included in this work for comparative purposes. In all cases, type IV N_2 adsorption desorption isotherms with an H1 hysteresis loop associated with capillary condensation in mesopores were obtained [20]. The catalysts had similar surface areas (45–53 m^2 g^{-1}), pore volumes (0.24–0.31 cm^3 g^{-1}), and a narrow pore size distribution with average pore diameters in the range 23–29 nm (Table 1). The XRD patterns of the catalysts only revealed diffraction peaks characteristic of the anatase phase. The crystallite size of anatase, determined by the Scherrer equation using the (101) diffraction peak [21], was in the range 22–23 nm (Table 1). In all cases, in accordance with the XRD results, the Raman spectra showed bands attributed solely to the presence of anatase at ca.144 cm^{-1} (E_g), 197 cm^{-1} (E_g), 399 cm^{-1} (B_{1g}), 515 cm^{-1} ($A_{1g} + B_{1g}$) and 639 cm^{-1} (E_g) [22].

The band-gap values were determined by UV–vis diffuse reflectance spectroscopy. The Kubelka-Munk formalism was used to convert the reflectance into the equivalent absorption coefficient, $F(R_\infty)$, and the band-gap values were calculated using the Tauc plot, $(F(R_\infty) \cdot h\upsilon)^n$ versus $h\upsilon$, where $n = 1/2$ denotes an indirect allowed transition [21]. The band-gap values of the catalysts were smaller than that of the bare TiO_2 anatase, 3.20 eV [13], with the decrease slightly greater for the catalysts containing Ga (Table 1). SEM-EDX images of the $Pt/Ga-TiO_2$ catalysts after calcination indicated that Ga and Pt species were quite homogeneously distributed over the anatase. As an example, the images corresponding to $Pt/0.2Ga-TiO_2$ are shown in Fig. 1.
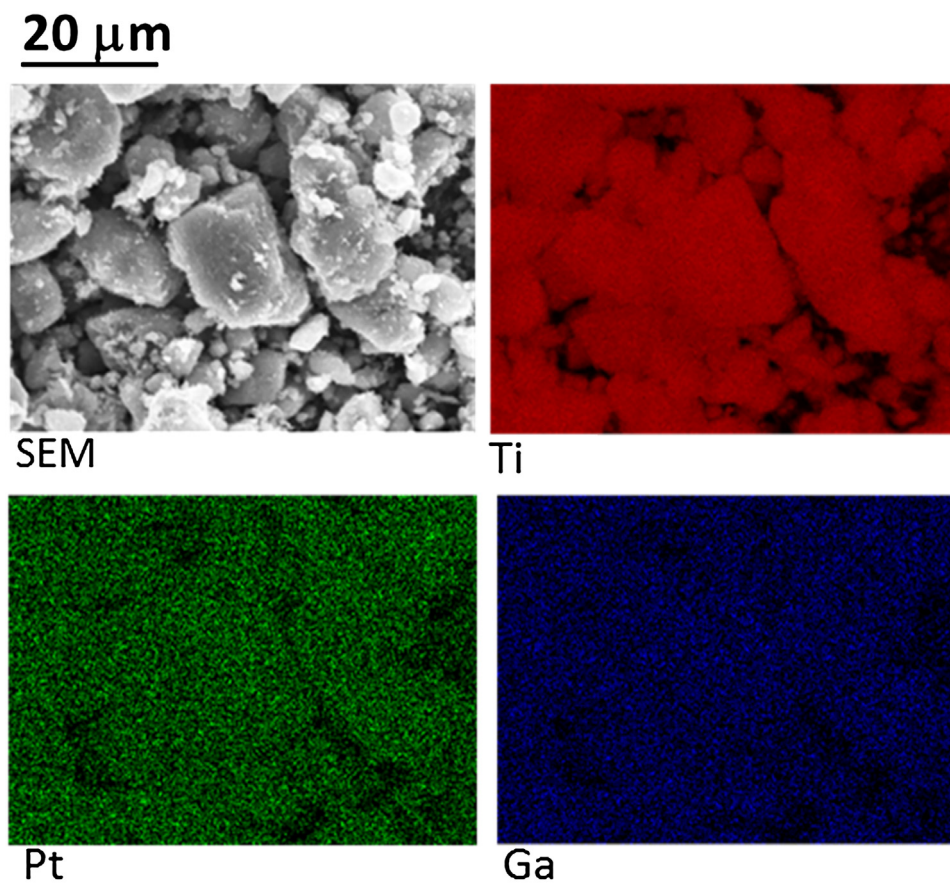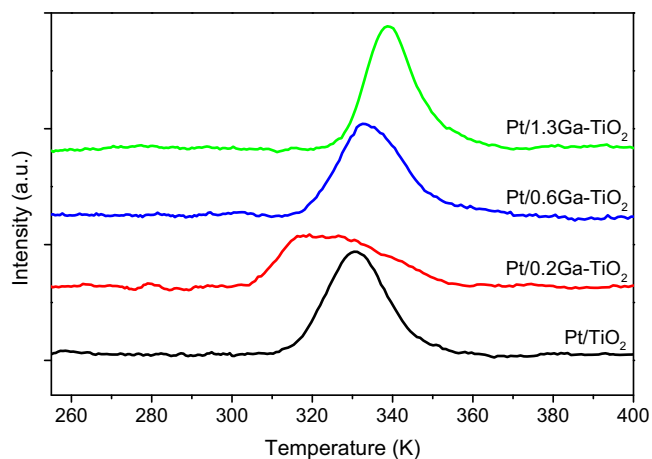
The reducibility properties of the catalysts were studied by H_2-TPR experiments. Fig. 2 shows the H_2 consumption profiles. For all the $Pt/Ga-TiO_2$ catalysts, a wide and asymmetric peak of H_2 consumption was observed; the corresponding maximum was located at higher temperatures as the content of Ga in the catalysts increased. The $Pt/0.2Ga-TiO_2$ and Pt/TiO_2 catalysts consumed 1.7 mol H_2/mol Pt; this value is lower than that necessary for reducing all the Pt species to Pt^0 if the presence of PtO_2 is considered (2 mol H_2/mol Pt). This is probably due to the partial decomposition of PtO_2 during calcination giving rise to PtO and/or Pt^0 [23]. The hydrogen consumption started at a lower temperature for $Pt/0.2Ga-TiO_2$ than for Pt/TiO_2 and the asymmetry of the peak corresponding to $Pt/0.2Ga-TiO_2$ contrasts with the symmetric peak observed for Pt/TiO_2; the presence of very small amounts of Ga clearly modified the reducibility of the Pt species. The H_2 consumption for $Pt/1.3Ga-TiO_2$ and $Pt/0.6Ga-TiO_2$ was 3 and 3.2 mol H_2/mol Pt, respectively. We associate this excessive H_2 consumption with partial reduction of $aGa-TiO_2$ ($a = 1.3, 0.6$).

The calcined catalysts were also analysed by XPS; Ti 2p, O 1s, Ga 2p and Pt 4f core-level spectra were recorded (Fig. 3). In all cases, the Ti 2p$_{3/2}$ peaks were centred at 458.7 eV and attributed

Table 1
Several characteristics of calcined Pt/TiO$_2$ and Pt-aGa/TiO$_2$ catalysts. Crystallite size (D) of anatase; BET surface-area (S$_{BET}$), pore volume (V$_{pore}$), and average pore diameter (D$_{pore}$); Band-gap and Pt and Ga weight percentage.

Catalyst	D (nm)	S$_{BET}$ (m^2 g^{-1})	V$_{pore}$ (cm^3 g^{-1})	D$_{pore}$ (nm)	Band-gap (eV)	% wt	
						Pt	Ga
Pt/TiO$_2$	22[a]	53[a]	0.31	29[a]	3.18	0.49[a]	–
Pt/0.2Ga-TiO$_2$	23	46	0.24	23	3.14	0.51	0.19
Pt/0.6Ga-TiO$_2$	23	46	0.24	23	3.15	0.47	0.61
Pt/1.3Ga-TiO$_2$	23	45	0.24	23	3.15	0.45	1.26

[a] From [19].

Fig. 1. SEM image and Ti, Pt and Ga distribution determined by EDX of the fresh Pt/0.2Ga-TiO$_2$ catalyst.

Fig. 2. H$_2$ consumption as a function of the temperature for Pt/Ga-TiO$_2$ and Pt/TiO$_2$ catalysts.

to Ti^{4+}; while the peaks corresponding to the O 1 s level showed a maximum at 529.9-530.1 eV, related with surface oxide species, and a small contribution at around 531.0 eV, characteristic of surface OH groups [24]. All the Pt/Ga-TiO$_2$ catalysts presented a peak corresponding to the Ga 2p$_{3/2}$ level centred at 1118.2 eV, which is associated with Ga^{3+} (Ga$_2$O$_3$). In all cases, the BE corresponding to the Pt 4f$_{7/2}$ level was 72.6 eV, characteristic of the presence of PtO$_x$ surface species.

The Pt/1.3Ga-TiO$_2$ catalyst showed wider Ti 2p$_{3/2}$, Pt 4f$_{7/2}$, Ga 2p$_{3/2}$ and O1s, peaks than the other catalysts (Fig. 3). The shoulder at 457.0 eV (Ti 2p$_{3/2}$) is associated with Ti^{3+} species [25]. The Pt 4f$_{7/2}$, Ga 2p$_{3/2}$ and O 1 s peaks of Pt/1.3Ga-TiO$_2$ also showed a shoulder in the zone of lower BE; this is related to the presence of Pt, Ga and oxide species with different electronic density and/or environment.

From the XPS spectra and the corresponding sensitivity factors, the (Pt/(Ti + Ga))$_{XPS}$ atomic ratios were calculated (Table 2). These ratios were higher for Pt/Ga-TiO$_2$ than for Pt/TiO$_2$, indicating greater Pt dispersion in the former. Moreover, this ratio increased when the Ga content decreased from 1.3 to 0.2%wt. Table 2 also shows the (Ga/Ti)$_{XPS}$ ratios of the Pt/Ga-TiO$_2$ catalysts; this ratio

Table 2
Pt dispersion and Pt particle size determined by CO chemisorption, (Pt/Ti + Ga) atomic ratio determined by ICP and surface atomic ratios determined by XPS.

Catalyst	Pt dispersion (%)	Pt (nm)	$(Pt/Ti+Ga)_{ICP}$	$Pt/(Ti+Ga)_{XPS}$		$Ga/(Ti)_{XPS}$ Fresh
				Fresh	Post-reaction	
Pt/TiO_2	52	2.2	0.0020	0.0111	0.0065[a]	–
$Pt/1.3Ga-TiO_2$	55	2.1	0.0018	0.0131	0.0091[b]	0.1376
$Pt/0.6Ga-TiO_2$	83	1.4	0.0019	0.0152	0.0152[a]	0.0683
$Pt/0.2Ga-TiO_2$	75	1.5	0.0021	0.0183	0.0152[a]	0.0142

[a] Reaction time 24 h.
[b] Reaction time 4 h.

increases with increasing Ga content in the $Pt/Ga-TiO_2$ catalysts. Fig. 4 shows the variation of $(Ga/Ti)_{XPS}$ with the Ga loading per nm^2 of $Pt/Ga-TiO_2$; an almost linear relationship between the parameters exists; the higher the theoretical Ga surface density (atoms Ga/nm^2), the higher the segregation of Ga species on the surface $((Ga/Ti)_{XPS})$.

The calcined catalysts were also characterized by CO chemisorption followed by DRIFTS. In all cases, after CO adsorption, a wide band in the $\upsilon(CO)$ zone was observed due to CO adsorption on different oxidized and reduced Pt sites (Fig. 5A). As indicated previously, during the calcination step partial decomposition of PtO_2 could take place and Pt^0 could coexist with oxidized Pt on the surface of the fresh catalysts. The $\upsilon(CO)$ bands of $Pt/0.2Ga-TiO_2$ and $Pt/0.6Ga-TiO_2$ can be deconvoluted into four components with maxima at $2105\,cm^{-1}$, $2084-2083\,cm^{-1}$, $2064-2062\,cm^{-1}$ and $2038-2035\,cm^{-1}$. The band at $2105\,cm^{-1}$ could be attributed to CO adsorbed on oxidized (111) Pt centres. CO adsorbed on reduced or oxidized Pt centres in different environments could contribute to the band at $2084-2083\,cm^{-1}$. The contribution of this band to the total $\upsilon(CO)$ band is less for $Pt/0.6Ga-TiO_2$ than for $Pt/0.2Ga-TiO_2$. The bands at $2064-2062\,cm^{-1}$ and $2038-2035\,cm^{-1}$ are associated with CO adsorbed at different Pt^0 sites [26–28]. Besides components at 2098, 2064 and $2027\,cm^{-1}$, the deconvolution of the $\upsilon(CO)$ corresponding to $Pt/1.3Ga-TiO_2$ shows a clear component at $2120\,cm^{-1}$ which is related to the presence of PtO_x species. A comparison of the $\upsilon(CO)$ bands in Fig. 5A indicates that the relative intensity of the bands due to CO coordinated on Pt^0 is higher in the spectra of catalysts containing Ga than in that of Pt/TiO_2.
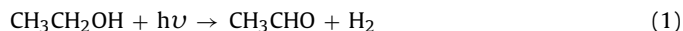
In an attempt to compare the catalysts as a function of their Pt dispersion, CO chemisorption experiments were carried out at 308 K over catalysts previously reduced at 398 K. For the calculation of the Pt dispersion and the size of the Pt particles, a stoichiometry for CO adsorption of one molecule of CO per surface Pt atom and the presence of cubic Pt particles were assumed. After reduction, the Pt dispersion in the $Pt/Ga-TiO_2$ catalysts was higher than in Pt/TiO_2 (Table 2); $Pt/0.2Ga-TiO_2$ and $Pt/0.6Ga-TiO_2$ showed a higher dispersion (75%–83% Pt dispersion) than $Pt/1.3Ga-TiO_2$ (55% Pt dispersion). Thus, the presence of a small amount of Ga favours Pt dispersion, in agreement with the XPS results concerning calcined catalysts discussed above. For Cu-based catalysts, the presence of Ga has also been shown to favour Cu dispersion, stabilizing the active phase [17].

3.2. Photocatalytic results

As stated in the experimental section, the photocatalytic production of H_2 from aqueous solutions of $ethanol_{(aq)}$ (25% v/v) was followed over time using $Pt/Ga-TiO_2$ catalysts. Fig. 6 shows the variation in the amount of H_2 produced as a function of reaction time for all $Pt/Ga-TiO_2$ catalysts. For comparative purposes, results corresponding to Pt/TiO_2 are also included in Fig. 6 [19]. $Pt/0.2Ga-TiO_2$ showed the highest initial rate of H_2 production ($0.54\,mmol\,min^{-1}$); but after 24 h of irradiation, it decreased by

about 75%. Although the profile of the H_2 production rate over time corresponding to $Pt/0.2Ga-TiO_2$ was similar to that of Pt/TiO_2, the deactivation of $Pt/0.2Ga-TiO_2$ was lower, and $Pt/0.2Ga-TiO_2$ showed a higher initial rate of H_2 production and a greater total amount of H_2 produced than Pt/TiO_2. $Pt/0.6Ga-TiO_2$ and $Pt/1.3Ga-TiO_2$ were initially less active than $Pt/0.2Ga-TiO_2$. This could be related to the progressive increase of the Ga/Ti ratio on the surface with the increase of Ga in the catalysts (Table 2 and Fig. 4). However, the deactivation of $Pt/0.6Ga-TiO_2$ and $Pt/1.3Ga-TiO_2$ was lower than that of $Pt/0.2Ga-TiO_2$. For $Pt/0.6Ga-TiO_2$, after 24 h of photocatalytic reaction, the rate of H_2 production was only 30% lower than initially.

Besides H_2, during the photocatalytic reaction, lower amounts of CO_2, CO, CH_4, C_2H_4 and C_2H_6 were produced in the gas phase. As for the liquid phase, the main product was acetaldehyde; smaller amounts of 2,3-butanediol, acetic acid and acetone were also produced. This indicates that in all cases, the main reaction which took place was the photocatalytic dehydrogenative oxidation of ethanol.

$$CH_3CH_2OH + h\upsilon \rightarrow CH_3CHO + H_2 \tag{1}$$

XPS characterization of the post-reaction catalysts indicated the presence of Pt^0 on the surface for all of them. Although the $(Pt/(Ti+Ga))_{XPS}$ atomic ratio of $Pt/0.2Ga-TiO_2$ and $Pt/1.3Ga-TiO_2$ decreased during the photocatalytic reaction, this diminution was less than that corresponding to Pt/TiO_2 (Table 2). It is worth mentioning that $Pt/0.6Ga-TiO_2$ showed a similar $(Pt/(Ti+Ga))_{XPS}$ ratio before and after the photocatalytic test; $Pt/0.6Ga-TiO_2$ also suffered a small decrease in the rate of production of H_2 over the 24 h photocatalytic test. Post-reaction catalysts were also characterized by CO chemisorption followed by DRIFTS; the corresponding spectra appear in Fig. 5B. In no case were there bands above $2100\,cm^{-1}$, this indicates that after the photocatalytic reaction, surface PtO_x species were not detected, in contrast with the results of CO chemisorption on the fresh catalysts (Fig. 5A). The $\upsilon(CO)$ bands obtained after the CO chemisorption onto the $Pt/Ga-TiO_2$ post-reaction catalysts were wide and their maxima were located at lower wavenumbers than that corresponding to post-reaction Pt/TiO_2; $2051-2048\,cm^{-1}$ compared to $2056\,cm^{-1}$ (Fig. 5B). Fig. 5B shows that the $\upsilon(CO)$ bands corresponding to post-reaction $Pt/Ga-TiO_2$ catalysts can be deconvoluted in four components with maxima at $2094-2080\,cm^{-1}$, $2055-2053\,cm^{-1}$, $2028-2027\,cm^{-1}$ and $1994-1980\,cm^{-1}$, which can be assigned to CO coordinated mostly on different Pt^0 sites with a high density of defects, such as edge and corner sites [29]. The lower wavenumber of the $\upsilon(CO)$ bands corresponding to post-reaction $Pt/Ga-TiO_2$ compared to post-reaction Pt/TiO_2 could indicate a dilution and/or electronic effect of Ga species on Pt ensembles [30,31].

4. Conclusions

The photocatalytic behaviour in production of H_2 from $ethanol_{(aq)}$ of $Pt/Ga-TiO_2$ catalysts (0.5%wt Pt, 0.2–1.3%wt Ga) differs from that of Pt/TiO_2 (0.5%wt Pt) and depends closely on the
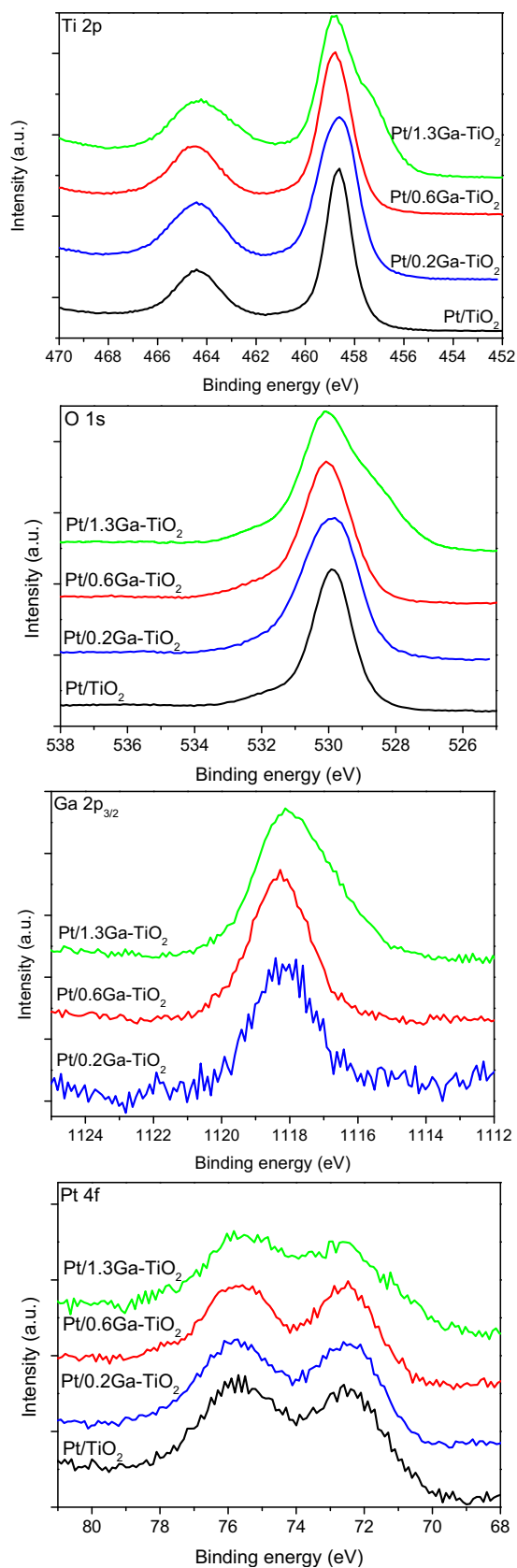
Fig. 3. XPS spectra corresponding to the Ti 2p, O 1s, Ga $2p_{3/2}$ and Pt 4f core levels of the Pt/Ga-TiO$_2$ and Pt/TiO$_2$ catalysts.
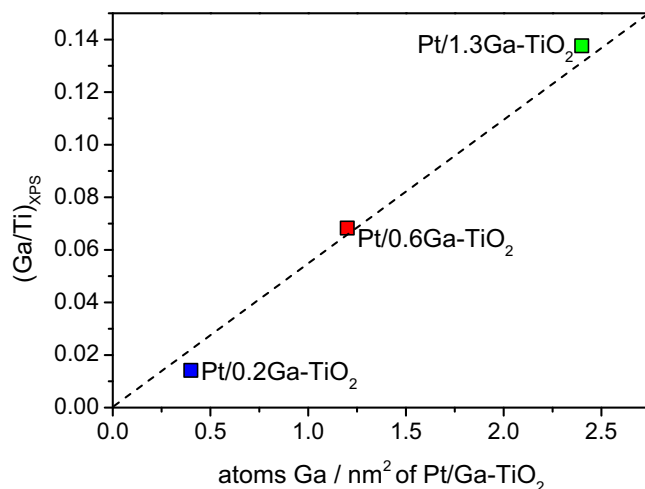

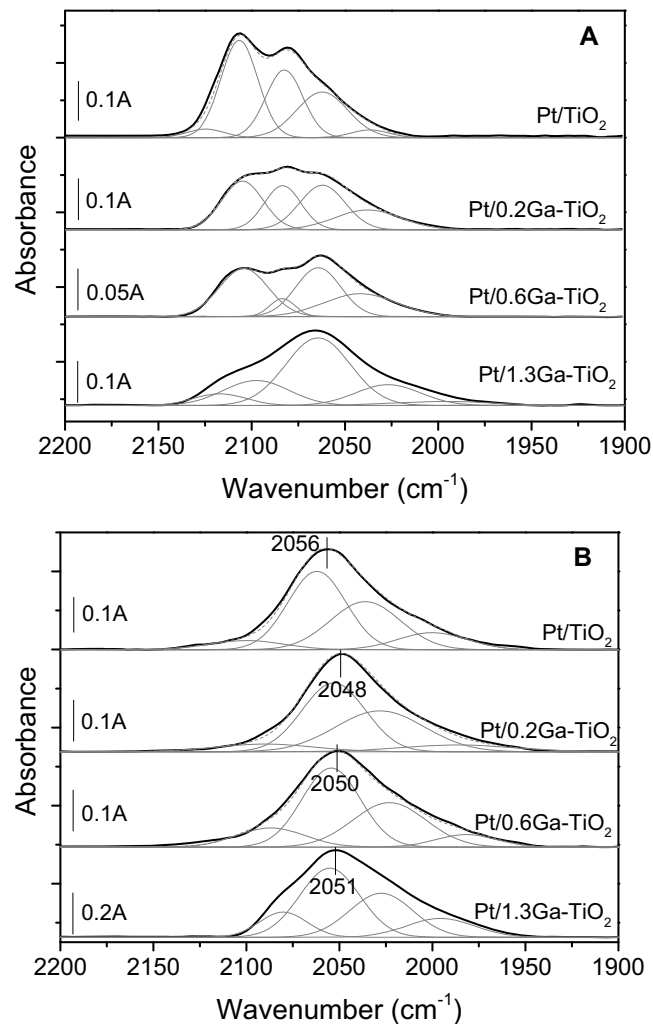Fig. 4. Relationship between the (Ga/Ti)$_{XPS}$ atomic ratio and the theoretical Ga surface density of the catalysts.

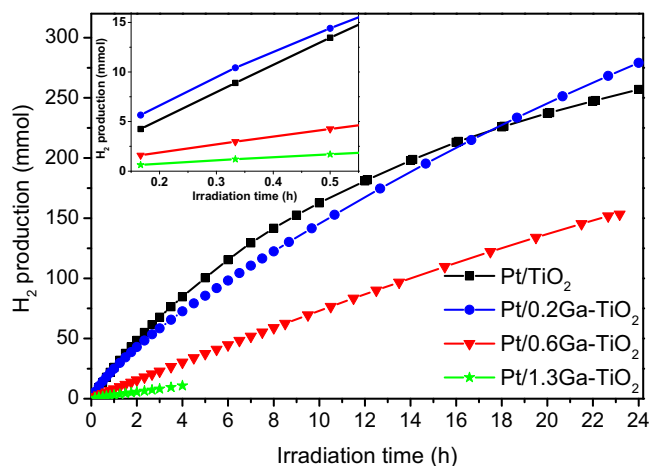Fig. 5. DRIFT spectra after CO adsorption over Pt/Ga-TiO$_2$ and Pt/TiO$_2$: A) fresh catalysts; B) post-reaction catalysts.

Fig. 6. Amount of H_2 produced as a function of the irradiation time over Pt/Ga-TiO$_2$ and Pt/TiO$_2$ catalysts. The inset shows an enlargement of the initial part of the graph.

Ga content of the catalyst. Fresh Pt/Ga-TiO$_2$ showed higher Pt dispersion and a lower relative amount of surface oxidized Pt species than fresh Pt/TiO$_2$. The decrease in the rate of hydrogen production during the photocatalytic reaction and the diminishing of Pt dispersion were less for Pt/Ga-TiO$_2$ catalysts than for Pt/TiO$_2$. Pt/0.2Ga-TiO$_2$ exhibited better photocatalytic performance than Pt/TiO$_2$. Pt/0.2Ga-TiO$_2$, with higher Pt dispersion than Pt/TiO$_2$, showed a higher initial rate of production of H_2 and produced a higher total amount of H_2. The initial rate of H_2 production of Pt/1.3Ga-TiO$_2$ was much lower than that of the other catalysts, and this could be related to an excess of Ga on the surface of the catalyst. The amount of H_2 produced by Pt/0.6Ga-TiO$_2$ was 50% of that produced by Pt/0.2Ga-TiO$_2$. However, Pt/0.6Ga-TiO$_2$ showed a quite stable behaviour during the photocatalytic test (24 h), and for this catalyst the surface Pt/(Ti + Ga) atomic ratio did not change during the photocatalytic reaction. Thus, a promoter effect of Ga related with the modification of surface Pt species is observed within the range 0.2–0.6%wt Ga content for the Pt/Ga-TiO$_2$ prepared in this work.

Acknowledgements

References

[1] N. Strataki, V. Bekiari, D.I. Kondarides, P. Lianos, Appl. Catal. B Environ. 77 (2007) 184–189.
[2] M. Cargnello, A. Gasparotto, V. Gombac, T. Montini, D. Barreca, P. Fornasiero, Eur. J. Inorg. Chem. (2011) 4309–4323.
[3] M. Bowker, Green Chem. 13 (2011) 2235–2246.
[4] V. Dal Santo, A. Gallo, A. Naldoni, M. Guidotti, R. Psaro, Catal. Today 197 (2012) 190–205.
[5] H. Lu, J. Zhao, L. Li, L. Gong, J. Zheng, L. Zhang, Z. Wang, J. Zhang, Z. Zhu, Energy Environ. Sci. 4 (2011) 3384–3388.
[6] G.R. Bamwenda, S. Tsubota, T. Nakamura, M. Haruta, J. Photochem, Photobiol. A Chem. 89 (1995) 177–189.
[7] R.M. Navarro, J. Arenales, F. Vaquero, I.D. González, J.L.G. Fierro, Catal. Today 210 (2013) 33–38.
[8] S. Escobedo Salas, B. Serrano Rosales, H. De Lasa, Appl. Catal. B Environ. 140–141 (2013) 523–536.
[9] C.R. López, E.P. Melián, J.A. Ortega Méndez, D.E. Santiago, J.M. Doña Rodríguez, O. González Díaz, J. Photochem. Photobiol. A Chem. 312 (2015) 45–54.
[10] M.P. Languer, F.R. Scheffer, A.F. Feil, D.L. Baptista, P. Migowski, G.J. Machado, D.P. De Moraes, J. Dupont, S.R. Teixeira, D.E. Weibel, Int. J. Hydrogen Energy 38 (2013) 14440–14450.
[11] A.L. Linsebigler, J.T. Yates Jr., G. Lu, Chem. Rev. 95 (1995) 735–758.
[12] D.Y.C. Leung, X. Fu, C. Wang, M. Ni, M.K.H. Leung, X. Wang, X. Fu, ChemSusChem 3 (2010) 681–694.
[13] K. Shimura, H. Yoshida, Energy Environ. Sci. 4 (2011) 2467–2481.
[14] X. Liu, M. Khan, W. Liu, W. Xiang, M. Guan, P. Jiang, W. Cao, Ceram. Int. 41 (2015) 3075–3080.
[15] S.S. Umare, A. Charanpahari, R. Sasikala, Mater. Chem. Phys. 140 (2013) 529–534.
[16] J. Llorca, P. Ramírez de la Piscina, J. León, J. Sales, J.L.G. Fierro, N. Homs, Stud. Surf. Sci. Catal. 130 (2000) 2513–2518.
[17] J. Toyir, P. Ramírez de la Piscina, J.L.G. Fierro, N. Homs, Appl. Catal. B Environ. 34 (2001) 255–266.
[18] A.C. Sola, D. Garzón Sousa, J. Araña, O. Gónzalez Díaz, J.M. Doña Rodríguez, P. Ramírez de la Piscina, N. Homs, Catal. Today 266 (2016) 53–61.
[19] A.C. Sola, N. Homs, P. Ramírez de la Piscina, Int. J. Hydrogen Energy 41 (2016) 19629–19636.
[20] M. Thommes, K. Kaneko, A.V. Neimark, J.P. Olivier, F. Rodriguez-Reinoso, J. Rouquerol, K.S.W. Sing, Pure Appl. Chem. 87 (2015) 1051–1069.
[21] D. Reyes-Coronado, G. Rodríguez-Gattorno, M.E. Espinosa-Pesqueira, C. Cab, R. de Coss, G. Oskam, Nanotechnology 19 (2008) 145605.
[22] J. Zhang, M. Li, Z. Feng, J. Chen, C. Li, J. Phys.Chem. B 110 (2006) 927–935.
[23] L.K. Ono, J.R. Croy, H. Heinrich, B.R. Cuenya, J. Phys. Chem. C 115 (2011) 16856–16866.
[24] H. Jensen, A. Soloviev, Z. Li, E.G. Søgaard, Appl. Surf. Sci. 246 (2005) 239–249.
[25] G. Liu, J. Pan, L. Yin, J.T. Irvine, F. Li, J. Tan, P. Wormald, H.M. Cheng, Adv. Funct. Mater. 22 (2012) 3233–3238.
[26] F. Coloma, J.M. Coronado, C.H. Rochester, J.A. Anderson, Catal. Lett. 51 (1998) 155–162.
[27] J. Ruiz-Martínez, A. Sepúlveda-Escribano, J.A. Anderson, F. Rodríguez-Reinoso, Phys. Chem.Chem. Phys. 11 (2009) 917–920.
[28] J. Silvestre-Albero, A. Sepúlveda-Escribano, F. Rodríguez-Reinoso, J.A. Anderson, J. Catal. 223 (2004) 179–190.
[29] K. Tanaka, J.M. White, J. Catal. 94 (1983) 81–94.
[30] M. Primet, J. Catal. 88 (1984) 273–282.
[31] J. Llorca, N. Homs, J. Araña, J. Sales, P. Ramírez de la Piscina, Appl. Surf. Sci. 134 (1998) 217–224.